Dominating Interlayer Resonant Energy Transfer in Type-II 2D Heterostructure

Arka Karmakar, Abdullah Al-Mahboob, Christopher E. Petoukhoff, Oksana Kravchyna, Nicholas S. Chan, Takashi Taniguchi, Kenji Watanabe, Keshav M. Dani*

AUTHOR ADDRESS

Corresponding Author

Arka Karmakar - Femtosecond Spectroscopy Unit, Okinawa Institute of Science and Technology Graduate University, 1919-1 Tancha, Onna, Kunigami District, Okinawa 904-0495, Japan

E-mail: arka.karmakar@oist.jp; karmakararka@gmail.com

Authors

Abdullah Al-Mahboob - Femtosecond Spectroscopy Unit, Okinawa Institute of Science and Technology Graduate University, 1919-1 Tancha, Onna, Kunigami District, Okinawa 904-0495, Japan

Christopher E. Petoukhoff - Femtosecond Spectroscopy Unit, Okinawa Institute of Science and Technology Graduate University, 1919-1 Tancha, Onna, Kunigami District, Okinawa 904-0495, Japan

Present Address: King Abdullah University of Science and Technology (KAUST), KAUST Solar Center (KSC), Physical Science and Engineering Division (PSE), Thuwal, 23955-6900, Kingdom of Saudi Arabia

Oksana Kravchyna - Femtosecond Spectroscopy Unit, Okinawa Institute of Science and Technology Graduate University, 1919-1 Tancha, Onna, Kunigami District, Okinawa 904-0495, Japan

Nicholas S. Chan - Femtosecond Spectroscopy Unit, Okinawa Institute of Science and Technology Graduate University, 1919-1 Tancha, Onna, Kunigami District, Okinawa 904-0495, Japan

Takashi Taniguchi - International Center for Materials Nanoarchitectonics, National Institute for Materials Science, 1-1 Namiki, Tsukuba, Ibaraki 305-0044, Japan

Kenji Watanabe - Research Center for Functional Materials, National Institute for Materials Science, 1-1 Namiki, Tsukuba, Ibaraki 305-0044, Japan

Keshav M. Dani - Femtosecond Spectroscopy Unit, Okinawa Institute of Science and Technology Graduate University, 1919-1 Tancha, Onna, Kunigami District, Okinawa 904-0495, Japan

ABSTRACT

Type-II heterostructures (HSs) are essential components of modern electronic and optoelectronic devices. Earlier studies have found that in type-II transition metal dichalcogenide (TMD) HSs, the dominating carrier relaxation pathway is the interlayer charge transfer (CT) mechanism. Here, this report shows that, in a type-II HS formed between monolayers of $MoSe_2$ and ReS_2, nonradiative energy transfer (ET) from higher to lower work function material (ReS_2 to $MoSe_2$) dominates over the traditional CT process with and *without* a charge-blocking interlayer. Without a charge-blocking interlayer, the HS area shows 3.6 times $MoSe_2$ photoluminescence (PL) enhancement as compared to the $MoSe_2$ area alone. In a completely encapsulated sample, the HS PL emission further increases by a factor of 6.4. After completely blocking the CT process, more than 1 order of magnitude higher $MoSe_2$ PL emission was achieved from the HS area. This work reveals that the nature of this ET is truly a resonant effect by showing that in a similar type-II HS formed by ReS_2 and WSe_2, CT dominates over ET, resulting in a severely quenched WSe_2 PL. This study not only provides significant insight into the competing interlayer processes but also shows an innovative way to increase the PL

emission intensity of the desired TMD material using ET process by carefully choosing the right material combination for HS.

KEYWORDS: energy transfer, charge transfer, photoluminescence, transition metal dichalcogenide, heterostructure

Energy transfer (ET) is a process in which energy is nonradiatively transferred from an excited fluorophore (donor) to another fluorophore (acceptor).[1–3] ET is a long-range process without involving emission and reabsorption of photons.[4] The ET theory is based on the concept considering an excited fluorophore as an oscillating dipole transferring energy to another dipole; similar as coupled pendulums in classical mechanics. We can use the following equation to describe the ET process from donor (D) to acceptor (A):

$$\boldsymbol{D}^* + \boldsymbol{A} \rightarrow \boldsymbol{D} + \boldsymbol{A}^* \qquad (1)$$

where D^* and A^* are the excited states of the fluorophores. When donor and acceptor are in close proximity and donor emission spectra overlaps with the acceptor absorption spectra, the excited state energy from the donor gets transferred to the acceptor *via* dipole-dipole interaction and subsequently released in the form of radiative energy emission from the acceptor.[2,3] ET, thus favorably occurs between parallel dipoles.[3] ET has already been proven as the building block of many biological and chemical applications.[5–8] Despite the long history of discovery,[1] ET exploration is still ongoing due to the fact that many promised applications are based on the idea of placing donor and acceptor in subnanometer proximity to fully utilize the ET process.[9]

Layered transition metal dichalcogenide (TMD) materials can be exfoliated down to atomically thin monolayers (1Ls), and the optical bandgaps of these materials spans the broad range of near-infrared to deep ultraviolet in the electromagnetic spectrum.[10] Subnanometer spacing in heterostructures (HSs) created by stacking different van der Waals (vdW) materials

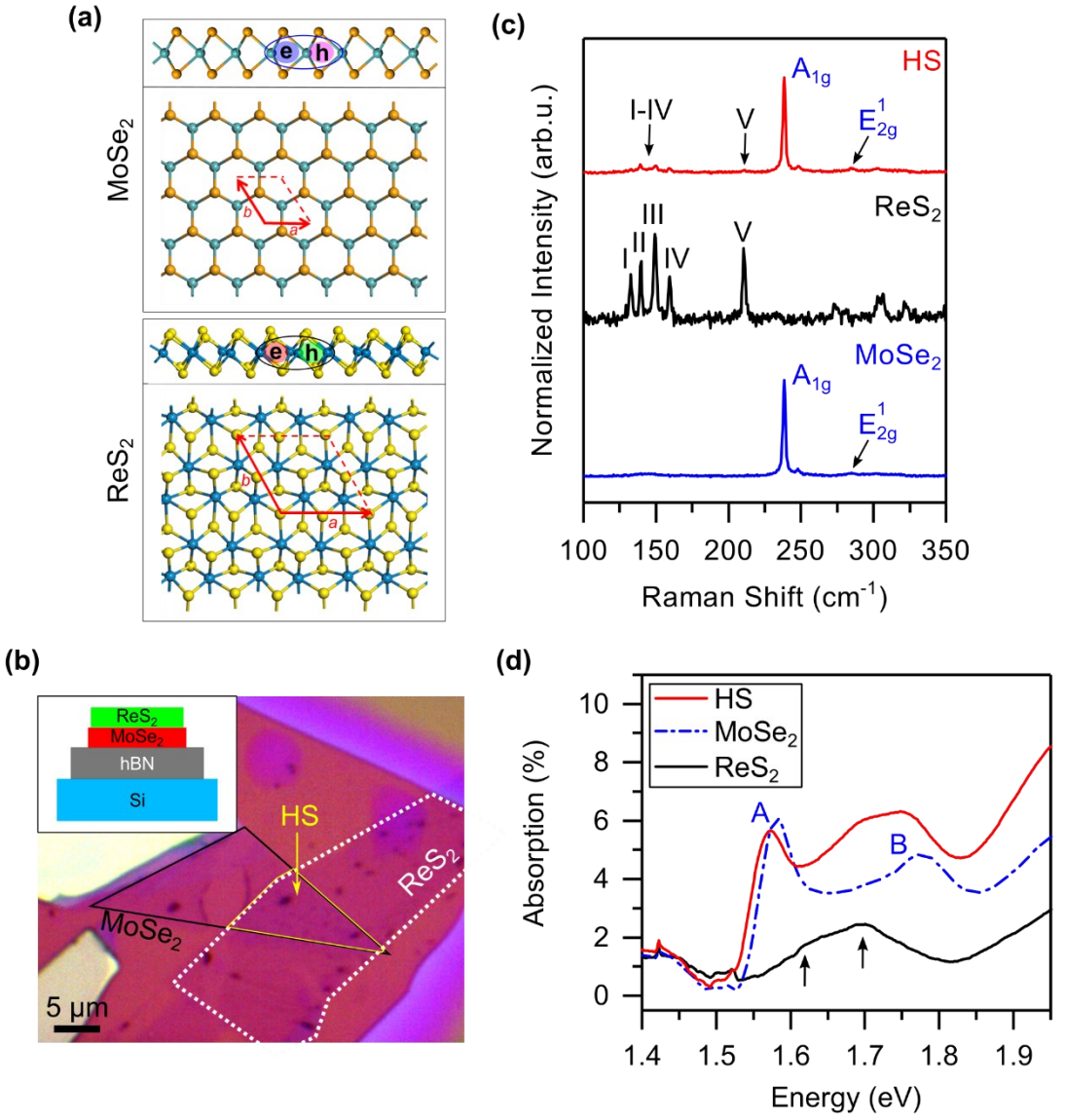

Figure 1. (a) Monolayer (1L) $MoSe_2$ and ReS_2 crystal structure. Top panels show the side view and bottom panels show the top view of the crystal structures. Side views show the schematic of in-plane orientation of dipoles across these layered materials. (b) Optical image of the ReS_2-$MoSe_2$ heterostructure from Sample 1 (S1). Inset is the schematic illustration of the sample's side view. (c) Raman spectra from the $MoSe_2$, ReS_2, and HS areas. HS Raman spectra consists of different vibrational modes from individual 1L area. (d) Absorption spectroscopy data of three different areas from a similar heterostructure made on a transparent sapphire substrate (Sample 2, S2). $MoSe_2$ A and B excitonic peaks are clearly visible, and ReS_2 lower energy absorption peaks are marked with arrows. HS spectra consists of peaks from both 1L areas.

has enabled opportunities to study exciting phenomena in 2D systems, such as Moiré patterns, valleytronics, spintronics and interlayer excitons just to mention a few.[11–14] Thus, TMD HSs are ideal candidates to study the ET process because they can be stacked in atomically close

proximity. In TMD HSs, interlayer energy and charge transfer (CT) compete with each other; thus, comprehensive understanding of these processes is necessary to develop TMD-based applications.

The majority of the available TMD materials form type-II HSs.[15] In traditional type-II TMD HSs, the dominating charge carrier relaxation pathway is interlayer CT process[16–18] rather than interlayer ET mechanism. Kozawa *et al*.[19] showed the presence of interlayer ET in type-II HS by placing an atomically thin charge-blocking layer, namely, a few-layer hexagonal boron nitride (hBN) in between the two TMD layers to suppress the interlayer CT process. Studying efficient ET process in TMD HSs requires materials with coinciding donor emission and acceptor absorption peak positions. Selection of the right TMD pairs is thus crucial to observing ET in type-II HSs.

A recent study[20] has predicted that a type-II HS formed between 1L rhenium disulfide (ReS_2) and 1L molybdenum diselenide ($MoSe_2$) integrated on a flexible substrate is an efficient candidate for near infrared (NIR) photodetection. Here, we experimentally study this HS and show that interlayer ET from ReS_2 to $MoSe_2$ dominates over the traditional interlayer CT process. As the donor, the emission of ReS_2 overlaps with the absorption of the acceptor, $MoSe_2$, and ReS_2 has a dominating nonradiative recombination channel. We show that the nonradiative ET from ReS_2 *resonantly* excites more carriers in $MoSe_2$ giving a 3.6 times enhanced PL emission from the HS even *without* having a charge-blocking layer in between the two materials. In a completely hBN encapsulated HS sample, we observe an increment of the HS PL emission by a factor of 6.4. By adding different thicknesses of hBN interlayer, we found that the PL enhancement, which is proportional to the ET, has a distance (d) dependence of $\sim 1/d^2$ at larger separation, indicating 2D dipole-2D dipole interaction between the TMD layers.[21–23] At a donor-acceptor separation of 13.5 nm, we successfully achieved 12.5 times higher $MoSe_2$ PL emission from the HS area by completely suppressing the other competing processes. We further show that, by replacing the $MoSe_2$ layer with 1L tungsten

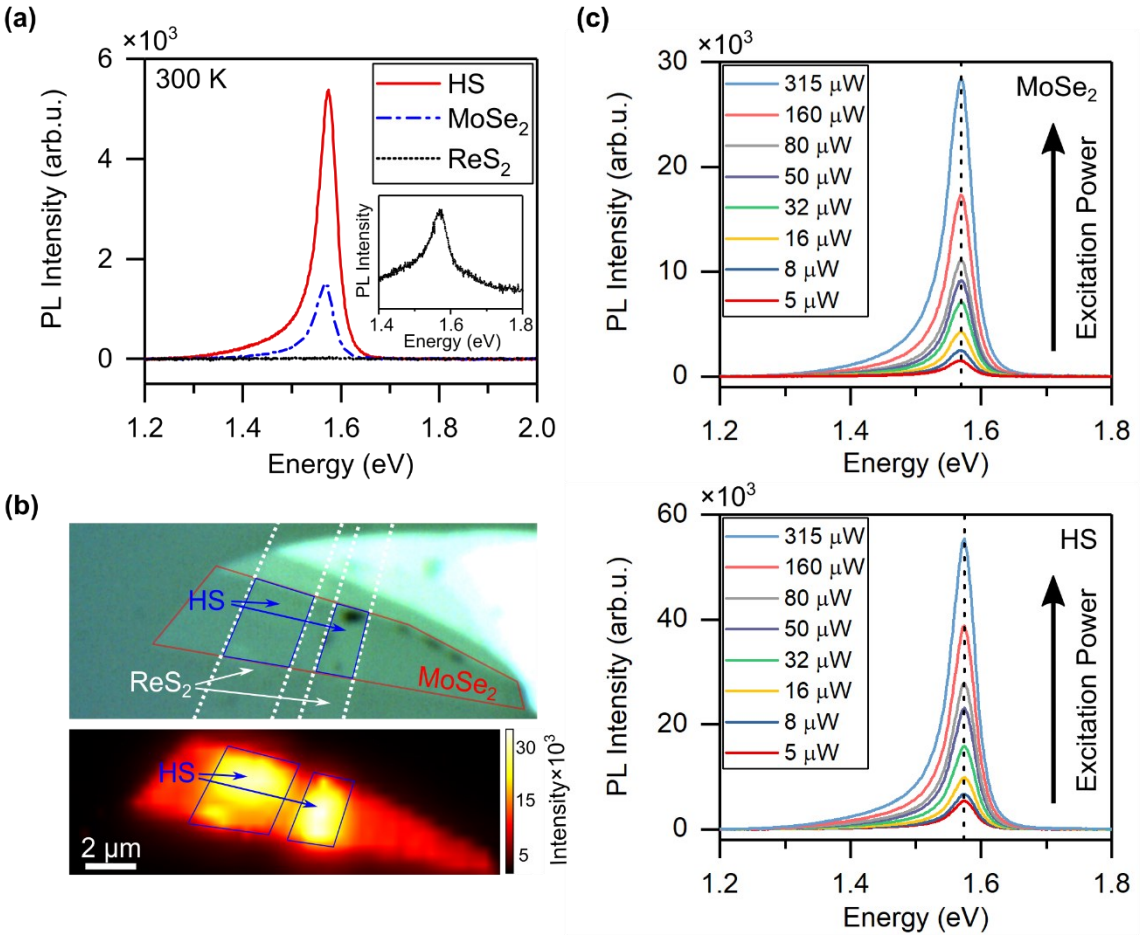

Figure 2. (a) Room temperature (RT) PL emission from the $MoSe_2$, ReS_2 and HS area of S1. Inset is the ReS_2 PL emission obtained at ~30 times higher laser power and longer accumulation. (b) Optical micrograph of another ReS_2-$MoSe_2$ HS, Sample 3 (S3) and PL intensity map from the same sample. The entire HS area shows this enhanced PL emission. (c) Laser power dependent PL from the $MoSe_2$ (top panel) and HS (bottom panel) area of S1. PL peak energy does not shift with increasing laser power, indicating that throughout the experiment we remain in material's linear regime.

diselenide (WSe_2), the resonant nature of ET breaks and interlayer CT dominates in the WSe_2-ReS_2 HS like other typical type-II HSs, exhibiting a severely quenched WSe_2 PL emission from the HS. This report shows that by carefully choosing the right material combination, we can interplay between the ET and CT processes and thus enhance the PL efficiency of the desired TMD material using resonant ET.

RESULTS AND DISCUSSION

The atomic arrangement of in-plane crystal structures of 1L $MoSe_2$ and 1L ReS_2 are shown in Figure 1(a), where the top and bottom panels of $MoSe_2$ (or ReS_2, respectively) show the side and top views of the materials. The side views also show the schematic illustration of the orientation of in-plane transition dipole moments in these layered materials. The $MoSe_2$ crystal structure has perfect in-plane 3-fold symmetry, whereas ReS_2 is an anisotropic material having triclinic crystal structure with an oblique in-plane lattice,[24,25] as shown in Figure 1(a). 1L ReS_2-1L $MoSe_2$ HS samples were fabricated using micromechanical exfoliation (see the *Experimental Details*) and were stacked onto thick hBN layers to eliminate any effect from surface-mediated trap states during our experiment. Figure 1(b) shows the optical micrograph of the fabricated 1L ReS_2-1L $MoSe_2$ HS on hBN/Si substrate, namely Sample 1 (hereafter S1), where the inset shows a schematic illustration of the cross-section (stacking of layers) of the fabricated sample. The representative Raman spectra (Figure 1(c)) from the three different areas on S1 show $MoSe_2$ characteristics A_{1g} and E^1_{2g} peaks,[26–28] ReS_2 intralayer modes (I-V),[29,30] and the HS Raman spectra consisting of the characteristic peaks from both materials. It is also worth to note that in the HS Raman spectra, the signature peak positions of each material remain the same as compared to the individual monolayer area, suggesting a similar level of doping and strain in the HS area as compared to the monolayer areas.[31,32] Figure 1(d) shows the absorption spectra from another HS made on a transparent sapphire substrate, Sample 2 (S2). We observed the characteristic A and B excitonic absorption from $MoSe_2$[19] as well as two identifying absorption peaks in ReS_2 within close proximity[33] (pointed with arrows in Figure 1(d)). HS absorption spectrum consists of peaks from each layer and showed an overall higher optical absorption as compared to the monolayer areas. The slight redshift in the HS absorption peaks as compared to the $MoSe_2$ area could be due to the change in electronic coupling and dielectric environment.[34,35] Room temperature (RT) PL peak position obtained from the $MoSe_2$ area of S1 matches well with previous published results[26,27,36] (Figure 2(a)). Being a pseudoindirect bandgap

semiconductor and having extremely low PL quantum yields, 1L ReS_2 has almost nonexistent PL emission[33,37,38] (Figure 2(a)). To obtain analyzable signal-to-noise ratio in the ReS_2 PL spectrum, the laser excitation power required was ~30 times higher, and the accumulation time was much longer compared to the $MoSe_2$ and HS areas (inset of Figure 2(a)). It is important to observe that at RT, ReS_2 PL emission and $MoSe_2$ excitonic absorption peak position almost *coincided* with each other around 1.60 eV. Such a coincidence between the nonradiative and radiative excitonic bandgaps enables resonant ET to dominate, as discussed in later sections. Although 1L ReS_2 had slightly lower absorption than 1L $MoSe_2$ (Figure 1(d)), the almost nonexistent PL emission further proved that nonradiative recombination dominated in the 1L ReS_2 film. The Raman peak positions and strong (weak) PL intensity of $MoSe_2$ (ReS_2) prove their monolayer nature. The HS PL peak position perfectly matched with the $MoSe_2$ PL peak position, but the luminescence from the HS area was enhanced by a factor of ~3.6 as compared to the PL emission from the area of $MoSe_2$ alone (Figure 2(a)). The enhancement factor considered here is the ratio of the HS PL peak intensity to the $MoSe_2$ peak intensity, when the two area are excited by the same low illumination intensity and accumulation time. In order to check the distribution of this enhanced PL emission over the HS area, we collected a PL intensity map on a similar ReS_2-$MoSe_2$ HS, namely Sample 3 (hereafter S3) (Figure 2(b)) (see S.I. Figure S1 for the PL spectra of the sample). The red area in Figure 2(b) corresponds to the 1L $MoSe_2$ area. From the PL map, it is clear that the PL enhancement was not a localized phenomenon, but the entire HS area showed this enhanced PL emission at RT. We note that, although the PL emission was non-uniform within the HS area, due to impurities, wrinkles, cracks, and defects forming at the material boundary during the vacuum-annealing, the PL emission from the HS area was always larger than that from the 1L $MoSe_2$.

To further investigate the origin of this enhanced PL emission from the HS (S1), we performed low temperature (LT) PL measurement at 100 K (Figure S2). At LT, the HS still

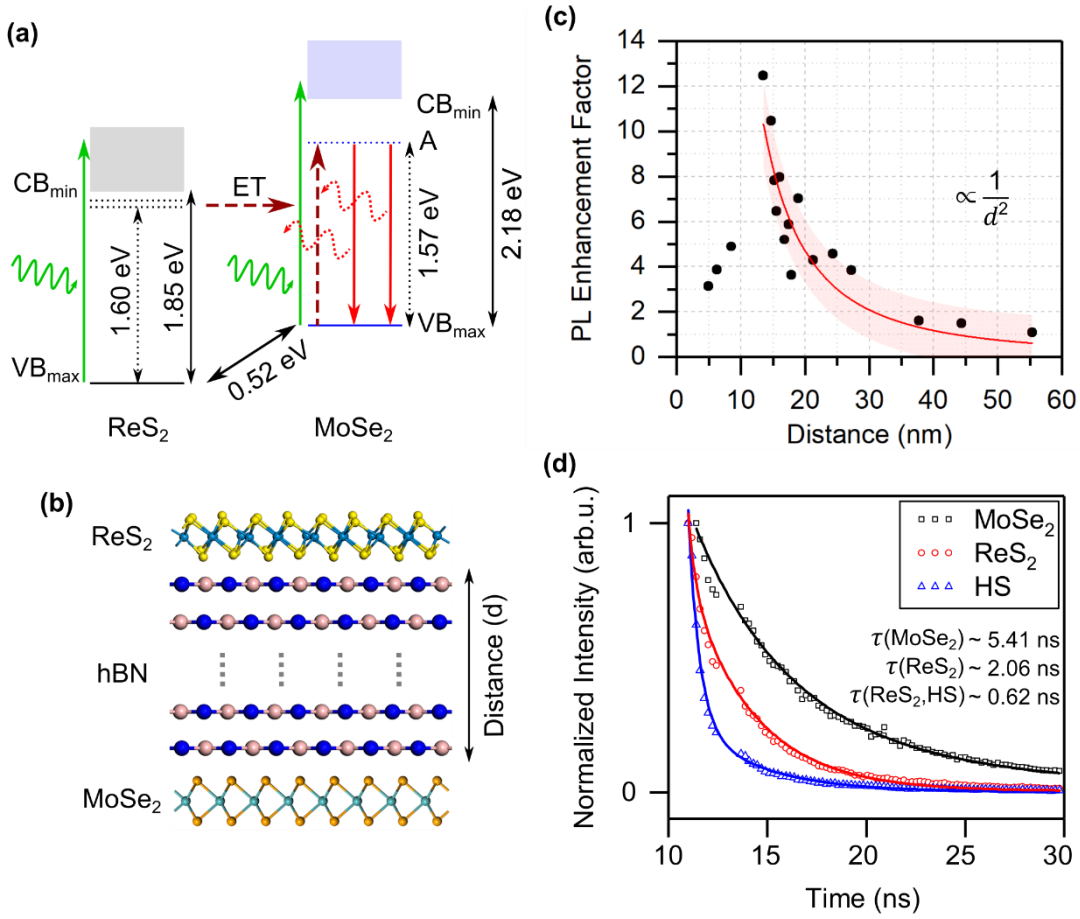

Figure 3. (a) Energy diagram representing the PL enhancement mechanism due to the resonance excitonic energy transfer from the ReS_2 to $MoSe_2$ layer. Excitonic levels are shown as dotted line below the conduction band minima. (b) Schematic illustration of the HS samples made with different thicknesses (distance) of hBN interlayer. (c) Change of PL enhancement from the HS area with distance. Pl enhancement factor shows $1/d^2$ dependency at larger separation. (d) RT time resolved PL (TR-PL) spectra from the $MoSe_2$, ReS_2, and HS area of S3. Curve fitted data are shown by the solid line.

showed a similar PL enhancement factor of ~3, indicating that weakly temperature dependent dipole-dipole coupling dominated in this HS rather than the Dexter-type ET process (interlayer exciton transfer).[19,39] Dexter- type ET can also be described using Equation 1, but the mechanism is different as discussed later. There is another possibility of the contribution of constructive interference from the back-reflected light at the sample-substrate interface as the origin of this enhanced PL emission.[40] However, we observed the HS PL enhancement in all of our samples irrespective of the different hBN substrate thicknesses, suggesting this interference was not a contributing factor. To further confirm this, we performed optical

transfer matrix method (TMM) calculations at different hBN thicknesses, and the results ruled out the possibility of any notable contribution from the optical interference effect in comparison to the observed PL enhancement (see S.I. for detailed discussion and Figure S3). Excitation power dependent PL measurements confirmed that we remained within the linear regimes of the materials (Figure 2(c)): for both the $MoSe_2$ and HS areas, the peak energy and full width at half maxima (FWHM) of the PL emission (Figure S4) remained unchanged with increasing excitation power. PL intensity shows sub-linear dependency with increasing laser power for both the $MoSe_2$ and HS area (Figure S5). This behavior suggests that defects/impurities affect the recombination mechanism in our samples,[41] which is typical for annealed, exfoliated TMD samples. To check the effect of dielectric screening as the origin of this PL enhancement[42] in the ReS_2-covered $MoSe_2$ layer, we fabricated an inverted $MoSe_2$-ReS_2 HS and observed similar PL enhancement (see Figure S6 for optical image and PL spectra of the sample), proving that dielectric screening had negligible effects in the PL enhancement process. After encapsulating the HS with a thin hBN top-layer, we further observed an overall increase in the HS PL emission by a factor of ~6.4 as compared to the encapsulated $MoSe_2$ area (Figure S7). We also exclude the possibilities of ET from hBN defects states[43] in our study (see S.I. for discussion and Figure S8-S9).

In order to experimentally determine the HS band-alignment type, we used Kelvin probe force microscopy (KPFM) to obtain the valence band (VB) offset (ΔE_V) between the $MoSe_2$ and ReS_2 layers as ~0.52 eV (Figure S10 and S11). Combining the experimental value of ΔE_V obtained from the KPFM measurement with the electronic bandgap,[44,45] we determined that 1L ReS_2-1L $MoSe_2$ HS indeed form a type-II band alignment (Figure 3(a)) in agreement with earlier published theoretical works.[15,20] This eliminated the possibility of short-range Dexter-type ET in our system, as it requires the complete exciton to be transferred from donor to acceptor, which can be accomplished in type-I HSs.[46] In typical type-II HSs, the PL emission of both materials quench after forming the HS due to the interlayer CT process.[16,17,19,47]

Interestingly the ReS_2-$MoSe_2$ HS, exhibited *enhanced* $MoSe_2$ PL emission from the HS area. We conclude that this enhancement was due to the ET process from the ReS_2 layer to the $MoSe_2$ layer. One possible reason of this unusual dominating ET process could be the suppression of coherent CT processes in this HS due to the weaker electronic coupling associated with symmetry mismatch and huge lattice mismatch between the trigonal in-plane of 2*H*-$MoSe_2$ and oblique in-plane of 1*T*-ReS_2 structure in comparison with the most studied 2*H*-TMD HSs. A recent ultrafast study on MoS_2-ReS_2 HS[48] showed much slower photocarrier transfer time on the order of 1 ps, as compared to the ~100 fs CT time in the HS formed between 2*H*-2*H* crystals.[17,49,50] However, the quantifiable reason for this dominating ET process remains unclear. Figure 3(a) shows the schematic illustration of the PL enhancement due to the proposed ET mechanism in the ReS_2-$MoSe_2$ HS. Upon photoexcitation with 2.33 eV (532 nm), hot excitons form above the bandgap, which thermalize to the lowest available excitonic level[45,51] and subsequently recombine at the VB releasing photons of the energy equal to the optical bandgap. In ReS_2, the majority of excited state carriers nonradiatively recombine to the VB *via* phonon-mediated processes. We propose the following mechanism to explain the PL enhancement: in the presence of weaker interlayer CT process, more carriers in $MoSe_2$ layer resonantly excite in the excitonic level due to excitonic ET from the ReS_2 layer, giving a significant excess of radiative excitons in $MoSe_2$. Thus, the $MoSe_2$ PL emission is enhanced in the HS as shown in Figure 3(a). We excluded the possibility of the ReS_2 PL enhancement in the HS due to the fact that the HS PL emission shape and peak position perfectly matched with the $MoSe_2$ PL spectra (Figure S12).

To understand the nature of the ET process, we made several HSs with varying thickness of hBN layers inserted between the TMD layers (Figure 3(b) and S13). ET shows a distance dependence between the donor and acceptor as $1/d^n$, where n is a factor dependent on the systems dimensionality:[52] n = 6 for 0D-to-0D dipole coupling, n = 4 for 0D-to-2D dipole coupling and n = 2 for 2D-to-2D dipole coupling.[21,22] It is important to mention that, at shorter

distances several processes such as charge tunneling through the hBN barrier, interlayer ET process and local impurity related opacity at the hBN-TMD interface could compete with each other. Thus, we considered to observe the pure ET effect from the maximum enhancement point in our experiment (Figure 3(c)). Specifically, at a distance of 13.5 and 14.7 nm we observed more than one order of magnitude higher PL enhancement factor of ~12.5 and 10.5, respectively. Beyond the maximum enhancement point, PL enhancement factor, which is considered to be directly proportional to ET, decreased with a ~$1/d^2$ dependency in our HS systems, which suggests that ET from ReS_2 to $MoSe_2$ occurred *via* 2D-to-2D dipole interaction.[21–23] The fluctuation observed in the data within 15-25 nm distance (Figure 3(c)) could be the combined effect of varying material's property from sample-to-sample and the change in coupling due to the rotational mismatch in our randomly stacked samples. We further confirmed the long-range dipole-dipole ET mechanism through a shortening of the excited state lifetime of the HS compared to the individual layers (Figure 3(d)). Compared to the isolated monolayers, which had PL lifetimes of ~ 5.41 and 2.06 ns for the acceptor ($MoSe_2$) and donor (ReS_2), respectively, the donor lifetime in the HS was shortened to ~620 ps (see *Experimental Details* and Table S1 in S.I. for the fitting details). ET occurs through a decreased donor fluorescence intensity and reduction of excited state lifetime accompanied by an increased acceptor fluorescence intensity. We find that there was a significant reduction of ReS_2 PL decay time in the HS as compared to the ReS_2 area alone (Figure 3(d)), which further proves that energy was transferred from ReS_2 to $MoSe_2$. To find the ET efficiency (E_{ET}) and ET rate (k_{ET}) in the ReS_2-$MoSe_2$ HS, we used the following equations:[4,53,54]

$$\boldsymbol{E_{ET} = 1 - \frac{\tau_{ReS2,HS}}{\tau_{ReS2}}} \quad (2)$$

$$\boldsymbol{k_{ET} = \frac{1}{\tau_{ReS2,HS}} - \frac{1}{\tau_{ReS2}}} \quad (3)$$

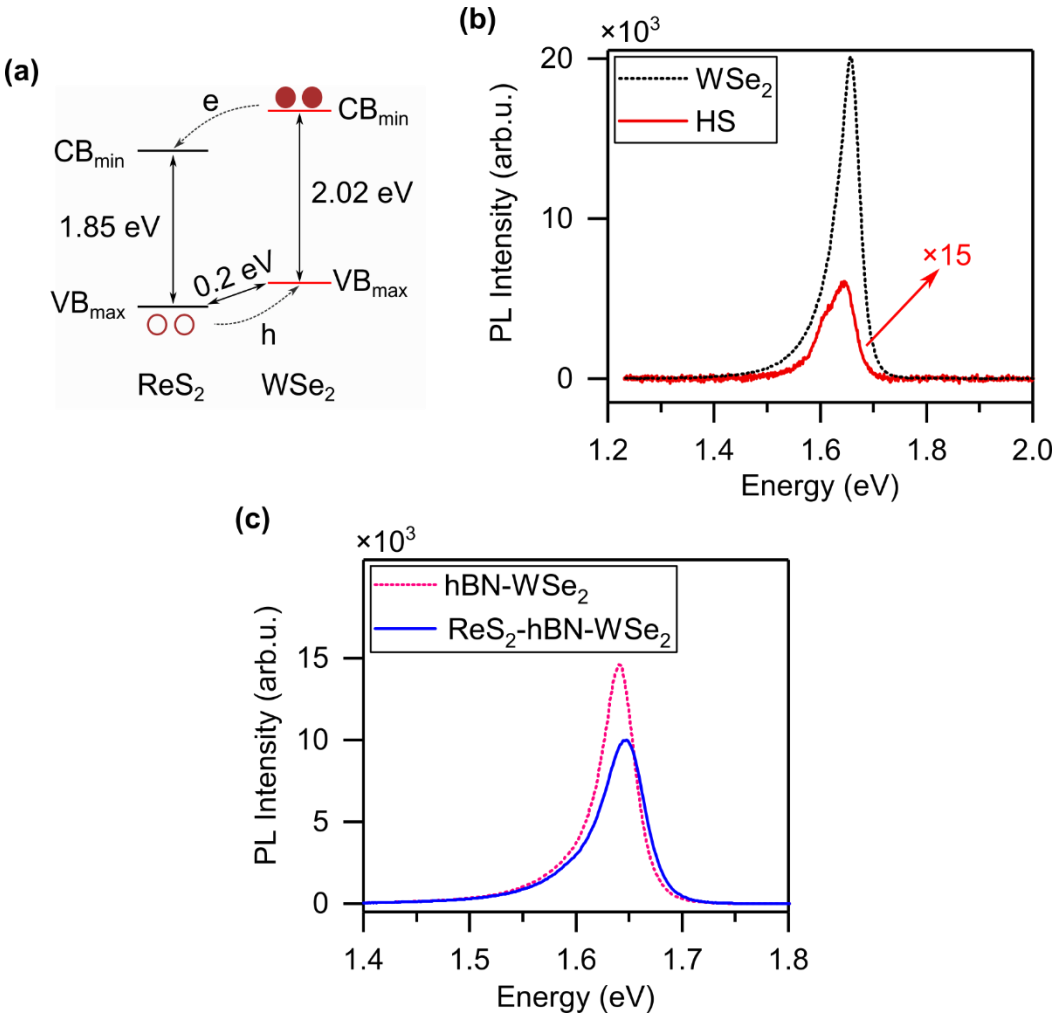

Figure 4. (a) Schematic illustration of type-II band alignment of ReS_2-WSe_2 HS. (b) PL measurement taken from the ReS_2-WSe_2 HS (Sample 4, S4) and 1L WSe_2 area. HS PL spectra shows massive quenching of WSe_2 emission. (c) PL spectra of the ReS_2-hBN-WSe_2 HS (Sample 5, S5) before and after transferring the top ReS_2 layer. After transferring the top ReS_2 layer, HS does not show an enhanced PL emission.

where $\tau_{ReS2,\,HS}$ is the ReS_2 PL lifetime in HS. By using the above-mentioned values in Equation 2 and 3 we calculate the ET efficiency and rate in the ReS_2-$MoSe_2$ HS to be ~70% and ~1.13 ns^{-1} respectively. Interestingly, only 70% E_{ET} due to the bright excitonic coupling cannot results in the observed 360% PL enhancement (and 640% for the hBN encapsulated sample). One possibility could be that the ReS_2 'short-lived' excitons are transferred before going through the nonradiative recombination process. Thus, the contribution from ReS_2 'short-lived' bright states in the ET process cannot be ignored.

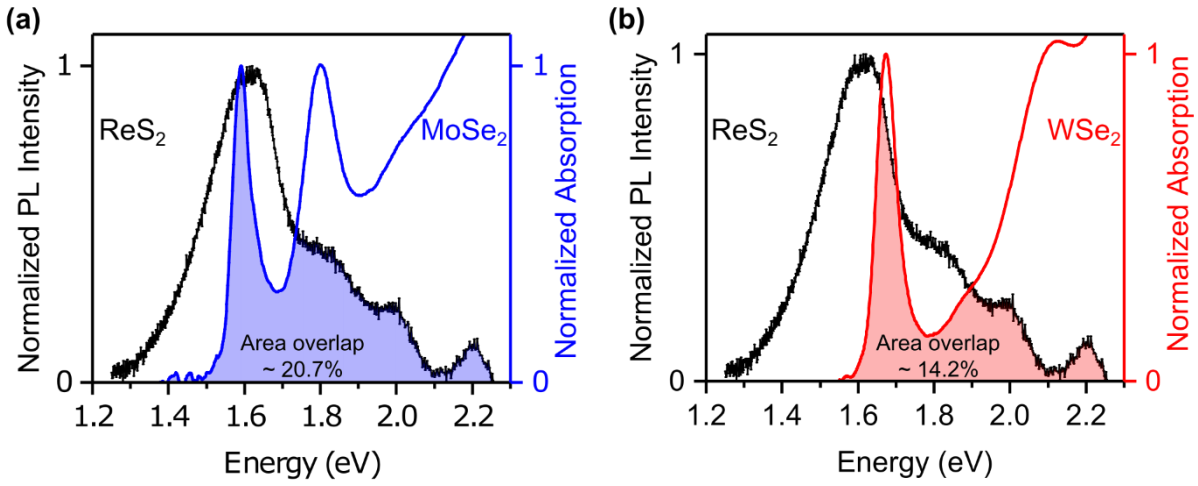

Figure 5. (a) and (b) Area overlaps between the normalized ReS_2 (donor) PL emission and the $MoSe_2$, WSe_2 (acceptor) absorption spectra at RT, respectively. The area overlaps for the $MoSe_2$ and WSe_2 system are ~20.7% and ~14.2%, respectively.

In order to check the resonant nature of the interlayer ET process, we replaced the $MoSe_2$ layer with WSe_2 (Sample 4, S4), which has about 80 meV larger optical bandgap than $MoSe_2$ (Figure 4 and S.I. Figure S14). The experimentally obtained ΔE_V between ReS_2 and WSe_2 from the KPFM measurement to be ~0.2 eV (Figure S15). Combining the ΔE_V value with WSe_2 electronic bandgap,[55] we found that 1L ReS_2-1L WSe_2 also form a similar type-II HS (Figure 4(a)), in agreement with previous reports.[15,20] PL measurements showed severely quenched HS PL emission (Figure 4(b)) due to interlayer CT being the dominant mechanism (Figure 4(a)), which is typical in type-II TMD HSs. It is worth mentioning here that in these ReS_2-$MoSe_2$ and ReS_2-WSe_2 HSs, the traditional type-II interlayer PL emissions are not visible due to the valley-forbidden dark excitonic nature (ReS_2 excitonic transition happens around the Γ valley in contrast with K valley in 2*H* materials).[20] To eliminate the interlayer CT process, we prepared a ReS_2-WSe_2 HS (Sample 5, S5) with few layers of hBN inserted in between. PL spectra of this HS did not lead to enhanced emission after placing the top ReS_2 layer (Figure 4(c)). The slightly reduced PL emission from the WSe_2 layer after placing the ReS_2 was mainly attributed to the absorption of the incoming photons from the top layer and scattering at the multiple interfaces. This was in stark contrast to the ReS_2-$MoSe_2$ and ReS_2-

hBN-$MoSe_2$ samples, where we observed PL enhancement regardless of the presence of the presence of a charge blocking hBN interlayer. It is evident that the ET from the ReS_2 layer was insufficient to enhance the PL emission from WSe_2 layer and the interlayer CT process dominated in this HS.

To further investigate the nature of the ET in TMDs, we examine the spectral overlap of the emission and absorption of donor and acceptors (Figure 5). The area overlaps for $MoSe_2$ and WSe_2 systems were ~20.7% and ~14.2%, respectively. It has been previously shown experimentally that E_{ET} increases with the increasing spectral overlap between the donor emission and acceptor absorption spectra.[56] Thus, based on the spectral overlaps, ET should be less efficient in the ReS_2-WSe_2 HS. However, the massive quenching of the WSe_2 PL emission from the HS proves that the ET rate cannot compete with the CT rate and donor relaxation rate in this configuration. This finally proves that nonradiative excitonic ET from ReS_2 *resonantly* excites radiative excitons in $MoSe_2$, resulting in the significant PL enhancement. This result also suggests that the traditional understanding may not be adequate enough to describe the ET process in these materials and future work will be required to develop a comprehensive understanding.

CONCLUSION

In summary, we have shown an interlayer resonant ET process in a type-II TMD HS *without* a charge blocking interlayer, resulting in 3.6 times $MoSe_2$ PL enhancement from the HS. We calculated the ET efficiency from our ReS_2-$MoSe_2$ HS to be ~70%, with a potential for increasing the overall efficiency in future work. The experimental findings suggest that resonant ET dominates over CT in ReS_2-$MoSe_2$ HSs, promoting radiative recombination in $MoSe_2$ at the HS region. Through insertion of a charge blocking hBN layer, we effectively suppress the competing CT process, achieving a maximum PL enhancement factor of 12.5 at a distance of 13.5 nm between the TMD layers. By varying the separation distance between

layers, we demonstrated the long-range ET has a distance dependence of ~$1/d^2$ for larger separation, indicating 2D dipole-to-2D dipole coupling between ReS_2 and $MoSe_2$ layers. Finally, we showed that by replacing the $MoSe_2$ layer with WSe_2, the resonant nature of ET broke, leading to interlayer CT dominating over the ET process, which resulted in a severely quenched WSe_2 PL emission from the HS. The ReS_2-$MoSe_2$ HS provides an opportunity to simultaneously study the ET and CT processes in TMD materials at ultrafast timescale in future work. We strongly believe that this work will help to discover more HS combinations that can exploit the normally parasitic nature of non-emissive 2D materials by increasing the PL emission intensity of 2D semiconducting emitters *via* ET, which can lead to improved TMD-based photovoltaic, optoelectronic, and photonic devices.

EXPERIMENTAL DETAILS

HS fabrication: hBN and TMD crystals were obtained from the National Institute of Materials Science, Japan; HQ Graphene, Netherlands and 2D Semiconductors, USA, respectively. hBN was exfoliated using the standard mechanical exfoliation technique. 1L TMD materials were exfoliated using the standard PDMS-based technique and carefully stacked on top of hBN flake using a homebuilt semi-automated transfer stage. ReS_2-$MoSe_2$ and ReS_2-WSe_2 HSs were annealed under high vacuum (~5×10^{-6} Torr) at 250 ºC for 4-6 hours to remove any polymer residue and make the monolayers in good contact with each other.

Characterization: For the **AFM** measurement, we used Bruker Dimension ICON3-OS1707 in 'ScanAsyst' (peak force tapping) mode to obtain the highest resolution AFM image.

We performed the **PL** and **Raman** spectroscopy measurement using Tokyo Instruments' Nanofinder 30 Microspectrometer. For low-temperature PL measurement the sample was loaded and cooled in a cryostat with continuous flow of liquid-nitrogen (N_2). For PL measurement the sample was illuminated using CW solid-state 532 nm laser with an average power of 5 μW (spot size ~1 μm) and focused by a 100x objective lens (N.A. 0.95).

For the **absorption** spectroscopy analysis, we used Craic 20/30 PV Microspectro-photometer system with white light illumination at perpendicular direction on the sample surface. The transmitted light passing through a variable aperture were collected using a 100x objective lens (N.A. 0.9) before entering to the spectrum analyzer. The transmission spectra was converted to absorption spectra using equation, $A\% = 100 - T\%$ (considering no reflection in the system).

We performed the **KPFM** measurement using the Bruker MultiMode 8 system with a platinum-iridium coated conductive tip. To obtain the high-resolution data we performed the measurement in frequency modulation (FM-KPFM) mode, which applies an AC voltage to the probe at very low frequency to obtain the electrostatic potential map of the sample surface.

TR-PL measurement was performed using a Spectra-Physics Matai XF-IMW femtosecond Ti:sapphire laser with tunable wavelengths from 710-920 nm, pulse width of 70 fs, and repetition rate of 80 MHz the 800 nm fundamental beam was passed through a second harmonic generator and pulse picker module to generate an excitation source with 400 nm wavelength and 4 MHz repetition rate. The spot size of the excitation beam on the sample surface was ~3 μm, with an average power of 90 μW. PL from the sample was collected through another 100x microscope objective (N.A. 0.70) and directed into a streak scope (Hamamatsu Photonics, C10627-03) coupled to a CCD. The instrument response function was determined by measuring the scattered laser light, which gave a temporal resolution of ~15 ps. After subtracting the instrumental response and the rise time, we fitted the normalized data from the $MoSe_2$ and ReS_2 monolayers area with a single-exponential decay function to get the faster decay component (intrinsic PL lifetime) . To obtain the ReS_2 lifetime in the HS, we fitted the HS data using the following equation:[57]

$$f(x) = A_1\,[exp(-(x-x_0)/\tau_{ReS2,HS}) - exp(-(x-x_0)/\tau_{MoSe2,HS})] + A_2\,[exp(-(x-x_o)/\tau_{MoSe2})]$$

where A_1, A_2 are constants, $\tau_{ReS2,HS}$ is the ReS_2 PL lifetime in the HS, $\tau_{MoSe2,HS}$ is the PL lifetime of excess charge in the HS $MoSe_2$ due to ET and τ_{MoSe2} is the $MoSe_2$ PL lifetime obtained from the 1L area.

AUTHOR INFORMATION

Author Contributions

A.K. conceived the project. A.K. and A.A.M. designed the experiments. A.K. fabricated the samples with help taken from O.K. and N.S.C. A.K. and A.A.M. characterized the samples. C.E.P. performed the TR-PL measurements and TMM calculations. K.M.D. provided the necessary funding. T.T. and K.W. provided the bulk hBN crystals for exfoliation. A.K. wrote the manuscript with feedback taken from all the co-authors.

Acknowledgements

A.K. acknowledges the useful discussion with Chakradhar Sahoo, and the help received from Joel Pérez Urquizo in setting up the cryo-PL measurements. This work was supported by the funding from the Femtosecond Spectroscopy Unit at the Okinawa Institute of Science and Technology Graduate University. K.W. and T.T. acknowledge support from the Elemental Strategy Initiative conducted by the MEXT, Japan (Grant Number JPMXP0112101001) and JSPS KAKENHI (Grant Numbers 19H05790 and JP20H00354).

ASSOCIATED CONTENT

Supporting Information Available: RT and LT PL spectra, details of TMM calculation, power dependent PL spectroscopy analysis, KPFM potential map and AFM height profile, Figure S1-S15; fitting parameters from the HS TR-PL data, Table S1.

Notes

The authors declare no competing financial interest.

REFERENCES

(1) Förster, T. Energy Migration and Fluorescence. *J. Biomed. Opt.* **2012**, *17* (1), 011002.

(2) Koushik, S. V; Vogel, S. S. Energy Migration Alters the Fluorescence Lifetime of Cerulean: Implications for Fluorescence Lifetime Imaging Forster Resonance Energy Transfer Measurements. *J. Biomed. Opt.* **2008**, *13* (3), 1–9. https://doi.org/10.1117/1.2940367.

(3) Clegg, R. M. Fluorescence Resonance Energy Transfer. *Curr. Opin. Biotechnol.* **1995**, *6* (1), 103–110. https://doi.org/https://doi.org/10.1016/0958-1669(95)80016-6.

(4) Joseph R. Lakowicz. *Principles of Fluorescence Spectroscopy*; Lakowicz, J. R., Ed.; Springer US: Boston, MA, 2006. https://doi.org/10.1007/978-0-387-46312-4.

(5) Ma, L.; Yang, F.; Zheng, J. Application of Fluorescence Resonance Energy Transfer in Protein Studies. *J. Mol. Struct.* **2014**, *1077*, 87–100. https://doi.org/https://doi.org/10.1016/j.molstruc.2013.12.071.

(6) Szöllosi, J.; Nagy, P.; Sebestyén, Z.; Damjanovich, S.; Park, J. W.; Mátyus, L. Applications of Fluorescence Resonance Energy Transfer for Mapping Biological Membranes. *Rev. Mol. Biotechnol.* **2002**, *82* (3), 251–266. https://doi.org/https://doi.org/10.1016/S1389-0352(01)00041-1.

(7) Hong, S.; Samson, A. A. S.; Song, J. M. Application of Fluorescence Resonance Energy Transfer to Bioprinting. *TrAC Trends Anal. Chem.* **2020**, *122*, 115749. https://doi.org/https://doi.org/10.1016/j.trac.2019.115749.

(8) Wu, L.; Huang, C.; Emery, B. P.; Sedgwick, A. C.; Bull, S. D.; He, X. P.; Tian, H.; Yoon, J.; Sessler, J. L.; James, T. D. Förster Resonance Energy Transfer (FRET)-Based Small-Molecule Sensors and Imaging Agents. *Chem. Soc. Rev.* **2020**, *49* (15), 5110–5139. https://doi.org/10.1039/C9CS00318E.

(9) Bradac, C.; Xu, Z. Q.; Aharonovich, I. Quantum Energy and Charge Transfer at Two-

Dimensional Interfaces. *Nano Lett.* **2021**, *21* (3), 1193–1204. https://doi.org/10.1021/acs.nanolett.0c04152.

(10) Gupta, S.; Shirodkar, S. N.; Kutana, A.; Yakobson, B. I. In Pursuit of 2D Materials for Maximum Optical Response. *ACS Nano* **2018**, *12* (11), 10880–10889. https://doi.org/10.1021/acsnano.8b03754.

(11) Zhang, C.; Chuu, C. P.; Ren, X.; Li, M. Y.; Li, L. J.; Jin, C.; Chou, M. Y.; Shih, C. K. Interlayer Couplings, Moiré Patterns, and 2D Electronic Superlattices in MoS2/WSe2 Hetero-Bilayers. *Sci. Adv.* **2017**, *3* (1). https://doi.org/10.1126/sciadv.1601459.

(12) Rivera, P.; Yu, H.; Seyler, K. L.; Wilson, N. P.; Yao, W.; Xu, X. Interlayer Valley Excitons in Heterobilayers of Transition Metal Dichalcogenides. *Nat. Nanotechnol.* **2018**, *13* (11), 1004–1015. https://doi.org/10.1038/s41565-018-0193-0.

(13) Miller, B.; Steinhoff, A.; Pano, B.; Klein, J.; Jahnke, F.; Holleitner, A.; Wurstbauer, U. Long-Lived Direct and Indirect Interlayer Excitons in van Der Waals Heterostructures. *Nano Lett.* **2017**, *17* (9), 5229–5237. https://doi.org/10.1021/acs.nanolett.7b01304.

(14) Han, W. Perspectives for Spintronics in 2D Materials. *APL Mater.* **2016**, *4* (3), 32401. https://doi.org/10.1063/1.4941712.

(15) Özcelik, V. O.; Azadani, J. G.; Yang, C.; Koester, S. J.; Low, T. Band Alignment of Two-Dimensional Semiconductors for Designing Heterostructures with Momentum Space Matching. *Phys. Rev. B* **2016**, *94* (3), 35125. https://doi.org/10.1103/PhysRevB.94.035125.

(16) Wang, K.; Huang, B.; Tian, M.; Ceballos, F.; Lin, M. W.; Mahjouri-Samani, M.; Boulesbaa, A.; Puretzky, A. A.; Rouleau, C. M.; Yoon, M.; Zhao, H.; Xiao, K.; Duscher, G.; Geohegan, D. B. Interlayer Coupling in Twisted WSe2/WS2 Bilayer Heterostructures Revealed by Optical Spectroscopy. *ACS Nano* **2016**, *10* (7), 6612–6622. https://doi.org/10.1021/acsnano.6b01486.

(17) Ceballos, F.; Bellus, M. Z.; Chiu, H. Y.; Zhao, H. Ultrafast Charge Separation and

Indirect Exciton Formation in a MoS2–MoSe2 van Der Waals Heterostructure. *ACS Nano* **2014**, *8* (12), 12717–12724. https://doi.org/10.1021/nn505736z.

(18) Peng, B.; Yu, G.; Liu, X.; Liu, B.; Liang, X.; Bi, L.; Deng, L.; Sum, T. C.; Loh, K. P. Ultrafast Charge Transfer in MoS 2 /WSe 2 p–n Heterojunction. *2D Mater.* **2016**, *3* (2), 25020. https://doi.org/10.1088/2053-1583/3/2/025020.

(19) Kozawa, D.; Carvalho, A.; Verzhbitskiy, I.; Giustiniano, F.; Miyauchi, Y.; Mouri, S.; Castro Neto, A. H.; Matsuda, K.; Eda, G. Evidence for Fast Interlayer Energy Transfer in MoSe2/WS2 Heterostructures. *Nano Lett.* **2016**, *16* (7), 4087–4093. https://doi.org/10.1021/acs.nanolett.6b00801.

(20) Saha, D.; Varghese, A.; Lodha, S. Atomistic Modeling of van Der Waals Heterostructures with Group-6 and Group-7 Monolayer Transition Metal Dichalcogenides for Near Infrared/Short-Wave Infrared Photodetection. *ACS Appl. Nano Mater.* **2020**, *3* (1), 820–829. https://doi.org/10.1021/acsanm.9b02342.

(21) Lin, T. N.; Huang, L. T.; Shu, G. W.; Yuan, C. T.; Shen, J. L.; Lin, C. A. J.; Chang, W. H.; Chiu, C. H.; Lin, D. W.; Lin, C. C.; Kuo, H. C. Distance Dependence of Energy Transfer from InGaN Quantum Wells to Graphene Oxide. *Opt. Lett.* **2013**, *38* (15), 2897–2899. https://doi.org/10.1364/OL.38.002897.

(22) Itskos, G.; Heliotis, G.; Lagoudakis, P. G.; Lupton, J.; Barradas, N. P.; Alves, E.; Pereira, S.; Watson, I. M.; Dawson, M. D.; Feldmann, J.; Murray, R.; Bradley, D. D. C. Efficient Dipole-Dipole Coupling of Mott-Wannier and Frenkel Excitons in (Ga,In)N Quantum Well/Polyfluorene Semiconductor Heterostructures. *Phys. Rev. B* **2007**, *76* (3), 35344. https://doi.org/10.1103/PhysRevB.76.035344.

(23) Taghipour, N.; Hernandez Martinez, P. L.; Ozden, A.; Olutas, M.; Dede, D.; Gungor, K.; Erdem, O.; Perkgoz, N. K.; Demir, H. V. Near-Unity Efficiency Energy Transfer from Colloidal Semiconductor Quantum Wells of CdSe/CdS Nanoplatelets to a Monolayer of MoS2. *ACS Nano* **2018**, *12* (8), 8547–8554.

https://doi.org/10.1021/acsnano.8b04119.

(24) Liu, E.; Fu, Y.; Wang, Y.; Feng, Y.; Liu, H.; Wan, X.; Zhou, W.; Wang, B.; Shao, L.; Ho, C. H.; Huang, Y. S.; Cao, Z.; Wang, L.; Li, A.; Zeng, J.; Song, F.; Wang, X.; Shi, Y.; Yuan, H.; Hwang, H. Y.; Cui, Y.; Miao, F.; Xing, D. Integrated Digital Inverters Based on Two-Dimensional Anisotropic ReS2 Field-Effect Transistors. *Nat. Commun.* **2015**, *6* (1), 6991. https://doi.org/10.1038/ncomms7991.

(25) Wolverson, D.; Crampin, S.; Kazemi, A. S.; Ilie, A.; Bending, S. J. Raman Spectra of Monolayer, Few-Layer, and Bulk ReSe2: An Anisotropic Layered Semiconductor. *ACS Nano* **2014**, *8* (11), 11154–11164. https://doi.org/10.1021/nn5053926.

(26) Tongay, S.; Suh, J.; Ataca, C.; Fan, W.; Luce, A.; Kang, J. S.; Liu, J.; Ko, C.; Raghunathanan, R.; Zhou, J.; Ogletree, F.; Li, J.; Grossman, J. C.; Wu, J. Defects Activated Photoluminescence in Two-Dimensional Semiconductors: Interplay between Bound, Charged and Free Excitons. *Sci. Rep.* **2013**, *3* (1), 2657. https://doi.org/10.1038/srep02657.

(27) Tonndorf, P.; Schmidt, R.; Böttger, P.; Zhang, X.; Börner, J.; Liebig, A.; Albrecht, M.; Kloc, C.; Gordan, O.; Zahn, D. R. T.; Michaelis de Vasconcellos, S.; Bratschitsch, R. Photoluminescence Emission and Raman Response of Monolayer MoS2, MoSe2, and WSe2. *Opt. Express* **2013**, *21* (4), 4908–4916. https://doi.org/10.1364/OE.21.004908.

(28) Mohamed, N. B.; Lim, H. E.; Wang, F.; Koirala, S.; Mouri, S.; Shinokita, K.; Miyauchi, Y.; Matsuda, K. Long Radiative Lifetimes of Excitons in Monolayer Transition-Metal DichalcogenidesMX2(M= Mo, W;X= S, Se). *Appl. Phys. Express* **2017**, *11* (1), 15201. https://doi.org/10.7567/apex.11.015201.

(29) Feng, Y.; Zhou, W.; Wang, Y.; Zhou, J.; Liu, E.; Fu, Y.; Ni, Z.; Wu, X.; Yuan, H.; Miao, F.; Wang, B.; Wan, X.; Xing, D. Raman Vibrational Spectra of Bulk to Monolayer ReS2 with Lower Symmetry. *Phys. Rev. B* **2015**, *92* (5), 54110. https://doi.org/10.1103/PhysRevB.92.054110.

(30) Chenet, D. A.; Aslan, O. B.; Huang, P. Y.; Fan, C.; van der Zande, A. M.; Heinz, T. F.; Hone, J. C. In-Plane Anisotropy in Mono- and Few-Layer ReS2 Probed by Raman Spectroscopy and Scanning Transmission Electron Microscopy. *Nano Lett.* **2015**, *15* (9), 5667–5672. https://doi.org/10.1021/acs.nanolett.5b00910.

(31) Yang, A.; Blancon, J. C.; Jiang, W.; Zhang, H.; Wong, J.; Yan, E.; Lin, Y. R.; Crochet, J.; Kanatzidis, M. G.; Jariwala, D.; Low, T.; Mohite, A. D.; Atwater, H. A. Giant Enhancement of Photoluminescence Emission in WS2-Two-Dimensional Perovskite Heterostructures. *Nano Lett.* **2019**, *19* (8), 4852–4860. https://doi.org/10.1021/acs.nanolett.8b05105.

(32) He, Z.; Xu, W.; Zhou, Y.; Wang, X.; Sheng, Y.; Rong, Y.; Guo, S.; Zhang, J.; Smith, J. M.; Warner, J. H. Biexciton Formation in Bilayer Tungsten Disulfide. *ACS Nano* **2016**, *10* (2), 2176–2183. https://doi.org/10.1021/acsnano.5b06678.

(33) Aslan, O. B.; Chenet, D. A.; van der Zande, A. M.; Hone, J. C.; Heinz, T. F. Linearly Polarized Excitons in Single- and Few-Layer ReS2 Crystals. *ACS Photonics* **2016**, *3* (1), 96–101. https://doi.org/10.1021/acsphotonics.5b00486.

(34) Raja, A.; Chaves, A.; Yu, J.; Arefe, G.; Hill, H. M.; Rigosi, A. F.; Berkelbach, T. C.; Nagler, P.; Schüller, C.; Korn, T.; Nuckolls, C.; Hone, J.; Brus, L. E.; Heinz, T. F.; Reichman, D. R.; Chernikov, A. Coulomb Engineering of the Bandgap and Excitons in Two-Dimensional Materials. *Nat. Commun.* **2017**, *8* (1), 15251. https://doi.org/10.1038/ncomms15251.

(35) Rigosi, A. F.; Hill, H. M.; Li, Y.; Chernikov, A.; Heinz, T. F. Probing Interlayer Interactions in Transition Metal Dichalcogenide Heterostructures by Optical Spectroscopy: MoS2/WS2 and MoSe2/WSe2. *Nano Lett.* **2015**, *15* (8), 5033–5038. https://doi.org/10.1021/acs.nanolett.5b01055.

(36) Le, C. T.; Clark, D. J.; Ullah, F.; Senthilkumar, V.; Jang, J. I.; Sim, Y.; Seong, M. J.; Chung, K. H.; Park, H.; Kim, Y. S. Nonlinear Optical Characteristics of Monolayer

MoSe2. *Ann. Phys.* **2016**, *528* (7–8), 551–559. https://doi.org/10.1002/andp.201600006.

(37) Tongay, S.; Sahin, H.; Ko, C.; Luce, A.; Fan, W.; Liu, K.; Zhou, J.; Huang, Y. S.; Ho, C. H.; Yan, J.; Ogletree, D. F.; Aloni, S.; Ji, J.; Li, S.; Li, J.; Peeters, F. M.; Wu, J. Monolayer Behaviour in Bulk ReS2 Due to Electronic and Vibrational Decoupling. *Nat. Commun.* **2014**, *5* (1), 3252. https://doi.org/10.1038/ncomms4252.

(38) Mohamed, N. B.; Shinokita, K.; Wang, X.; Lim, H. E.; Tan, D.; Miyauchi, Y.; Matsuda, K. Photoluminescence Quantum Yields for Atomically Thin-Layered ReS2: Identification of Indirect-Bandgap Semiconductors. *Appl. Phys. Lett.* **2018**, *113* (12), 121112. https://doi.org/10.1063/1.5037116.

(39) Tomita, A.; Shah, J.; Knox, R. S. Efficient Exciton Energy Transfer between Widely Separated Quantum Wells at Low Temperatures. *Phys. Rev. B* **1996**, *53* (16), 10793–10803. https://doi.org/10.1103/PhysRevB.53.10793.

(40) Dandu, M.; Biswas, R.; Das, S.; Kallatt, S.; Chatterjee, S.; Mahajan, M.; Raghunathan, V.; Majumdar, K. Strong Single- and Two-Photon Luminescence Enhancement by Nonradiative Energy Transfer across Layered Heterostructure. *ACS Nano* **2019**, *13* (4), 4795–4803. https://doi.org/10.1021/acsnano.9b01553.

(41) Kaplan, D.; Mills, K.; Lee, J.; Torrel, S.; Swaminathan, V. Excitation Intensity Dependent Photoluminescence of Annealed Two-Dimensional MoS2 Grown by Chemical Vapor Deposition. *J. Appl. Phys.* **2016**, *119* (21), 214301. https://doi.org/10.1063/1.4948662.

(42) Lin, Y.; Ling, X.; Yu, L.; Huang, S.; Hsu, A. L.; Lee, Y. H.; Kong, J.; Dresselhaus, M. S.; Palacios, T. Dielectric Screening of Excitons and Trions in Single-Layer MoS2. *Nano Lett.* **2014**, *14* (10), 5569–5576. https://doi.org/10.1021/nl501988y.

(43) Li, C.; Xu, Z. Q.; Mendelson, N.; Kianinia, M.; Wan, Y.; Toth, M.; Aharonovich, I.; Bradac, C. Resonant Energy Transfer between Hexagonal Boron Nitride Quantum

Emitters and Atomically Layered Transition Metal Dichalcogenides. *2D Mater.* **2020**, *7* (4), 45015. https://doi.org/10.1088/2053-1583/aba332.

(44) Gehlmann, M.; Aguilera, I.; Bihlmayer, G.; Nemšák, S.; Nagler, P.; Gospodarič, P.; Zamborlini, G.; Eschbach, M.; Feyer, V.; Kronast, F.; Młyńczak, E.; Korn, T.; Plucinski, L.; Schüller, C.; Blügel, S.; Schneider, C. M. Direct Observation of the Band Gap Transition in Atomically Thin ReS2. *Nano Lett.* **2017**, *17* (9), 5187–5192. https://doi.org/10.1021/acs.nanolett.7b00627.

(45) Ugeda, M. M.; Bradley, A. J.; Shi, S. F.; da Jornada, F. H.; Zhang, Y.; Qiu, D. Y.; Ruan, W.; Mo, S. K.; Hussain, Z.; Shen, Z. X.; Wang, F.; Louie, S. G.; Crommie, M. F. Giant Bandgap Renormalization and Excitonic Effects in a Monolayer Transition Metal Dichalcogenide Semiconductor. *Nat. Mater.* **2014**, *13* (12), 1091–1095. https://doi.org/10.1038/nmat4061.

(46) Wu, L.; Chen, Y.; Zhou, H.; Zhu, H. Ultrafast Energy Transfer of Both Bright and Dark Excitons in 2D van Der Waals Heterostructures Beyond Dipolar Coupling. *ACS Nano* **2019**, *13* (2), 2341–2348. https://doi.org/10.1021/acsnano.8b09059.

(47) Yuan, J.; Najmaei, S.; Zhang, Z.; Zhang, J.; Lei, S.; Ajayan, P. M.; Yakobson, B. I.; Lou, J. Photoluminescence Quenching and Charge Transfer in Artificial Heterostacks of Monolayer Transition Metal Dichalcogenides and Few-Layer Black Phosphorus. *ACS Nano* **2015**, *9* (1), 555–563. https://doi.org/10.1021/nn505809d.

(48) Bellus, M. Z.; Li, M.; Lane, S. D.; Ceballos, F.; Cui, Q.; Zeng, X. C.; Zhao, H. Type-I van Der Waals Heterostructure Formed by MoS2 and ReS2 Monolayers. *Nanoscale Horiz.* **2017**, *2* (1), 31–36. https://doi.org/10.1039/C6NH00144K.

(49) Merkl, P.; Mooshammer, F.; Steinleitner, P.; Girnghuber, A.; Lin, K. Q.; Nagler, P.; Holler, J.; Schüller, C.; Lupton, J. M.; Korn, T.; Ovesen, S.; Brem, S.; Malic, E.; Huber, R. Ultrafast Transition between Exciton Phases in van Der Waals Heterostructures. *Nat. Mater.* **2019**, *18* (7), 691–696. https://doi.org/10.1038/s41563-

019-0337-0.

(50) Hong, X.; Kim, J.; Shi, S. F.; Zhang, Y.; Jin, C.; Sun, Y.; Tongay, S.; Wu, J.; Zhang, Y.; Wang, F. Ultrafast Charge Transfer in Atomically Thin MoS2/WS2 Heterostructures. *Nat. Nanotechnol.* **2014**, *9* (9), 682–686. https://doi.org/10.1038/nnano.2014.167.

(51) Park, Y.; Han, S. W.; Chan, C. C. S.; Reid, B. P. L.; Taylor, R. A.; Kim, N.; Jo, Y.; Im, H.; Kim, K. S. Interplay between Many Body Effects and Coulomb Screening in the Optical Bandgap of Atomically Thin MoS2. *Nanoscale* **2017**, *9* (30), 10647–10652. https://doi.org/10.1039/C7NR01834G.

(52) Barnes, W. L. Fluorescence near Interfaces: The Role of Photonic Mode Density. *J. Mod. Opt.* **1998**, *45* (4), 661–699. https://doi.org/10.1080/09500349808230614.

(53) Li, M.; Chen, J. S.; Cotlet, M. Efficient Light Harvesting Biotic–Abiotic Nanohybrid System Incorporating Atomically Thin van Der Waals Transition Metal Dichalcogenides. *ACS Photonics* **2019**, *6* (6), 1451–1457. https://doi.org/10.1021/acsphotonics.9b00090.

(54) Tanoh, A. O. A.; Gauriot, N.; Delport, G.; Xiao, J.; Pandya, R.; Sung, J.; Allardice, J.; Li, Z.; Williams, C. A.; Baldwin, A.; Stranks, S. D.; Rao, A. Directed Energy Transfer from Monolayer WS2 to Near-Infrared Emitting PbS–CdS Quantum Dots. *ACS Nano* **2020**, *14* (11), 15374–15384. https://doi.org/10.1021/acsnano.0c05818.

(55) He, K.; Kumar, N.; Zhao, L.; Wang, Z.; Mak, K. F.; Zhao, H.; Shan, J. Tightly Bound Excitons in Monolayer WSe2. *Phys. Rev. Lett.* **2014**, *113* (2), 26803. https://doi.org/10.1103/PhysRevLett.113.026803.

(56) Kowerko, D.; Krause, S.; Amecke, N.; Abdel-Mottaleb, M.; Schuster, J.; Von Borczyskowski, C. Identification of Different Donor-Acceptor Structures *via* Förster Resonance Energy Transfer (FRET) in Quantum-Dot-Perylene Bisimide Assemblies. *Int. J. Mol. Sci.* **2009**, *10* (12), 5239–5256. https://doi.org/10.3390/ijms10125239.

(57) Gu, J.; Liu, X.; Lin, E.; Lee, Y. H.; Forrest, S. R.; Menon, V. M. Dipole-Aligned Energy Transfer between Excitons in Two-Dimensional Transition Metal Dichalcogenide and Organic Semiconductor. *ACS Photonics* **2018**, *5* (1), 100–104. https://doi.org/10.1021/acsphotonics.7b00730.